



HAL
open science

Toward using collective x-ray Thomson scattering to study C–H demixing and hydrogen metallization in warm dense matter conditions

D. Ranjan, K. Ramakrishna, K. Voigt, O. Humphries, B. Heuser, M. Stevenson, J. Lütgert, Z. He, C. Qu, S. Schumacher, et al.

► To cite this version:

D. Ranjan, K. Ramakrishna, K. Voigt, O. Humphries, B. Heuser, et al.. Toward using collective x-ray Thomson scattering to study C–H demixing and hydrogen metallization in warm dense matter conditions. *Physics of Plasmas*, 2023, 30 (5), pp.052702. 10.1063/5.0146416 . hal-04308514

HAL Id: hal-04308514


<https://hal.science/hal-04308514>

Submitted on 27 Nov 2023

HAL is a multi-disciplinary open access archive for the deposit and dissemination of scientific research documents, whether they are published or not. The documents may come from teaching and research institutions in France or abroad, or from public or private research centers.

L'archive ouverte pluridisciplinaire **HAL**, est destinée au dépôt et à la diffusion de documents scientifiques de niveau recherche, publiés ou non, émanant des établissements d'enseignement et de recherche français ou étrangers, des laboratoires publics ou privés.

AUTHOR QUERY FORM

	<p>Journal: Phys. Plasmas</p> <p>Article Number: POP23-AR-00178</p>	<p>Please provide your responses and any corrections by annotating this PDF and uploading it to AIP's eProof website as detailed in the Welcome email.</p>
---	---	--

Dear Author,

Below are the queries associated with your article; please answer all of these queries before sending the proof back to AIP.

Article checklist: In order to ensure greater accuracy, please check the following and make all necessary corrections before returning your proof.

1. Is the title of your article accurate and spelled correctly?
2. Please check affiliations including spelling, completeness, and correct linking to authors.
3. Did you remember to include acknowledgment of funding, if required, and is it accurate?

Location in article	Query / Remark: click on the Q link to navigate to the appropriate spot in the proof. There, insert your comments as a PDF annotation.
AQ1	Please check that the author names are in the proper order and spelled correctly. Also, please ensure that each author's given and surnames have been correctly identified (given names are highlighted in red and surnames appear in blue).
AQ2	Please provide the publisher name for Ref. 9.
AQ3	Please verify the page number in Ref. 24, as we have inserted the required information.
AQ4	Please provide the complete details for Ref. 31.
AQ5	Please provide the report number for Ref. 55.
AQ6	<p>We were unable to locate a digital object identifier (doi) for Ref(s). 12. Please verify and correct author names and journal details (journal title, volume number, page number, and year) as needed and provide the doi. If a doi is not available, no other information is needed from you. For additional information on doi's, please select this link: http://www.doi.org/.</p> <p>Please confirm ORCID's are accurate. If you wish to add an ORCID for any author that does not have one, you may do so now. For more information on ORCID, see https://orcid.org/.</p> <p>D. Ranjan - 0000-0002-8641-4794</p> <p>K. Ramakrishna - 0000-0003-4211-2484</p> <p>K. Voigt - 0000-0001-8090-2626</p> <p>O. S. Humphries - 0000-0001-6748-0422</p> <p>B. Heuser - 0000-0001-6363-1780</p> <p>M. G. Stevenson-</p> <p>J. Lüttert - 0000-0002-2593-573X</p> <p>Z. He - 0000-0001-5416-456X</p> <p>C. Qu-</p>

S. Schumacher - 0000-0002-1846-0000
P. T. May - 0009-0003-4989-8704
A. Amouretti-
K. Appel - 0000-0002-2902-2102
E. Brambrink-
V. Cerantola - 0000-0002-2808-2963
D. Chekrygina - 0000-0002-7337-2337
L. B. Fletcher - 0000-0002-7120-7194
S. Göde-
M. Harmand - 0000-0003-0713-5824
N. J. Hartley - 0000-0002-6268-2436
S. P. Hau-Riege - 0000-0001-7331-6485
M. Makita - 0000-0003-1513-9198
A. Pelka-
A. K. Schuster - 0000-0001-5489-5952
M. Smid-
T. Toncian - 0000-0001-7986-3631
M. Zhang-
T. R. Preston - 0000-0003-1228-2263
U. Zastra - 0000-0002-3575-4449
J. Vorberger - 0000-0001-5926-9192
D. Kraus - 0000-0002-6350-4180

Please check and confirm the Funder(s) and Grant Reference Number(s) provided with your submission:

Helmholtz Association, Award/Contract Number VH-NG-1141

Helmholtz Association, Award/Contract Number ERC-RA-0041

Helmholtz Association, Award/Contract Number VH-NG-1338

Bundesministerium für Bildung und Forschung, Award/Contract Number

Sächsisches Staatsministerium für Wissenschaft und Kunst, Award/Contract Number

Fusion Energy Sciences, Award/Contract Number FWP 100182

Laboratory Directed Research and Development, Award/Contract Number DE-AC02-76SF00515

Lawrence Livermore National Laboratory, Award/Contract Number DE- AC52-07NA27344

GSI Helmholtzzentrum für Schwerionenforschung, Award/Contract Number GSI-URDK2224

Please add any additional funding sources not stated above:

Thank you for your assistance.

Toward using collective x-ray Thomson scattering to study C-H demixing and hydrogen metallization in warm dense matter conditions

Cite as: Phys. Plasmas **30**, 000000 (2023); doi: 10.1063/5.0146416

Submitted: 13 February 2023 · Accepted: 23 April 2023 ·

Published Online: 0 Month 0000



AQ1

D. Ranjan,^{1,2,a)} K. Ramakrishna,³ K. Voigt,^{1,4} O. S. Humphries,^{1,5} B. Heuser,^{1,2} M. G. Stevenson,² J. Lütgert,² Z. He,^{1,2,6} C. Qu,² S. Schumacher,² P. T. May,² A. Amouretti,⁷ K. Appel,⁵ E. Brambrink,⁵ V. Cerantola,⁵ D. Chekrygina,⁸ L. B. Fletcher,⁹ S. Göde,⁵ M. Harmand,⁷ N. J. Hartley,⁹ S. P. Hau-Riege,¹⁰ M. Makita,⁵ A. Pelka,¹ A. K. Schuster,^{1,4} M. Smid,¹ T. Toncian,¹ M. Zhang,^{1,11} T. R. Preston,⁵ U. Zastra,⁵ J. Vorberger,¹ and D. Kraus^{1,2,b)}

AFFILIATIONS

¹Helmholtz-Zentrum Dresden-Rossendorf, Bautzner Landstraße 400, 01328 Dresden, Germany

²Institut für Physik, Universität Rostock, 18051 Rostock, Germany

³Center for Advanced Systems Understanding (CASUS), Helmholtz-Zentrum Dresden-Rossendorf (HZDR), 02826 Görlitz, Germany

⁴Technische Universität Dresden, 01069 Dresden, Germany

⁵European XFEL GmbH, 22869 Schenefeld, Germany

⁶Shanghai Institute of Laser Plasma, 201800 Shanghai, China

⁷Institut de Minéralogie, de Physique des Matériaux et de Cosmochimie, Sorbonne Université, 75005 Paris, France

⁸Scientific Computing Department, Rutherford Appleton Laboratory, Science and Technology Facilities Council, Harwell Campus, Didcot OX11 0QX, United Kingdom

⁹SLAC National Accelerator Laboratory, Menlo Park, California 94309, USA

¹⁰Lawrence Livermore National Laboratory, Livermore, California 94550, USA

¹¹Institute of Physical Science and Information Technology, Anhui University, Hefei 230601, China

^{a)}Author to whom correspondence should be addressed: d.ranjan@hzdr.de

^{b)}Electronic mail: dominik.kraus@uni-rostock.de

ABSTRACT

The insulator–metal transition in liquid hydrogen is an important phenomenon to understand the interiors of gas giants, such as Jupiter and Saturn, as well as the physical and chemical behavior of materials at high pressures and temperatures. Here, the path toward an experimental approach is detailed based on spectrally resolved x-ray scattering, tailored to observe and characterize hydrogen metallization in dynamically compressed hydrocarbons in the regime of carbon–hydrogen phase separation. With the help of time-dependent density functional theory calculations and scattering spectra from undriven carbon samples collected at the European x-ray Free-Electron Laser Facility (EuXFEL), we demonstrate sufficient data quality for observing C–H demixing and investigating the presence of liquid metallic hydrogen in future experiments using the reprinted drive laser systems at EuXFEL.

© 2023 Author(s). All article content, except where otherwise noted, is licensed under a Creative Commons Attribution (CC BY) license (<http://creativecommons.org/licenses/by/4.0/>). <https://doi.org/10.1063/5.0146416>

I. INTRODUCTION

The first confirmed discovery of an exoplanet in 1992¹ and then the discovery of an exoplanet around a Sun-like star by Mayor and Queloz² opened the floodgates for the detection of exoplanets, leading to multiple dedicated missions to look for exoplanets across the galaxy.

After 30 years and over 5000 confirmed exoplanets,³ it is now increasingly important to understand how planetary systems form and evolve. A large number of discovered exoplanets lie in the range of masses of gas giants like Jupiter and Saturn and ice giants like Uranus and Neptune, with the ice giants dominating the population.^{4,5}

47 Studying these large bodies in our Solar System continues to enhance
48 our understanding of the formation and evolution of planetary sys-
49 tems in general.

50 Various probe missions afforded us extensive data and improved
51 our understanding of the planets by exploring the upper layers and
52 space around them. The interiors of these astrophysical bodies can be
53 constrained using the measurements of their physical properties, but
54 establishing the internal structure and their bulk composition requires
55 a better understanding of the behavior of the chemical species at high-
56 pressure and high-temperature conditions. The thermal energies at
57 planetary interior conditions are at the same order of magnitude as the
58 energies stored in the chemical bonds, resulting in expected complex
59 chemical processes including phase transitions, species separation, and
60 demixing.^{6,7} The chemical composition and potential chemical pro-
61 cesses taking place inside these planets are essential for creating better
62 models and understanding their thermal, magnetic, and electrical
63 properties.⁸

64 The deep planetary conditions are at the low-temperature end of
65 the warm dense matter (WDM) regime. WDM describes the transi-
66 tion region between cold condensed matter and high-temperature
67 plasmas.^{9,10} One of the materials with great interest in research at
68 WDM conditions is metallic hydrogen. It was first predicted by
69 Wigner and Huntington¹¹ that solid molecular hydrogen would trans-
70 form into metal at high pressures. A pressure-induced liquid–liquid
71 phase transition from molecular hydrogen to a metallic phase is rele-
72 vant to planetary interiors and therefore has been widely
73 researched.^{12–14} The transition is referred to as plasma phase transi-
74 tion, which, depending on temperature, is predicted to either be an
75 abrupt first-order phase transition or a continuous transition to the
76 metallic state.^{15–17}

77 Theoretical and experimental studies of metallic hydrogen have
78 significantly contributed to the current understanding of planetary
79 evolution. Jupiter and Saturn are predicted to have an interior domi-
80 nated by liquid metallic hydrogen, which is in contrast to the proper-
81 ties of the insulating, molecular form present in the outer layers.⁶ This
82 highly condensed metallic hydrogen in the interior of gas giant planets
83 is expected to be responsible for the strong dynamo that drives their
84 exceptionally strong magnetic fields.¹⁸ Uranus and Neptune are most
85 often modeled to be made of three layers: a rocky core consisting of sil-
86 icates and iron, an “icy” shell that contains a mixture of water, meth-
87 ane, and ammonia, and a gaseous envelope dominated by hydrogen
88 and helium.^{19–21} In the high-pressure and high-temperature environ-
89 ment of these icy-giant planets, it is predicted that methane will form
90 polymeric hydrocarbon chains^{8,22} and, deeper toward the core, will
91 dissociate into carbon in the form of diamond and metallic
92 hydrogen.^{23–26}

93 Transcribing the physics of WDM state requires consider-
94 ation of highly interacting particles. Coupling and quantum effects
95 are not perturbations in the WDM regime, but are as strong as the
96 thermal energy. The complex interplay of competing forces is a
97 reason that the precise theoretical modeling to adequately portray
98 the physics is very difficult.^{9,27,28} To test the models, dedicated lab-
99 oratory experiments need to be performed. The so-far applied
100 experimental methods are mostly based on cryogenic liquid hydro-
101 gen as the initial material and include static compression
102 approaches using diamond anvil cells^{29–32} and various dynamic
103 compression techniques.^{15,33–36}

In addition to the challenges of compressing hydrogen to metalli- 104
zation conditions using the above-mentioned methods, the complexity 105
of cryogenic sample environments to start with high-density hydrogen 106
from the beginning also limits diagnostic capabilities. The measure- 107
ment of electrical conductivities for liquid H₂ and D₂ dynamically 108
compressed by high-velocity impactors driven by a gun has provided 109
the first pioneering insight.³⁵ In more recent approaches, the insula- 110
tor–metal transition of hydrogen has been characterized by determin- 111
ing the surface reflectivity of the compressed sample. While there has 112
been progress using a surface reflectivity method, there are notable dis- 113
crepancies in the P–T conditions where hydrogen metallization was 114
observed.^{33,34} Indeed, systematic uncertainties of the approach arise 115
from the fact that the reflecting interface is often in direct contact with 116
a material containing the sample, which may induce additional chem- 117
istry and changes in the electronic structure. Therefore, techniques 118
capable of accessing the interior of the sample and probing the bulk 119
volume are preferable but difficult to realize experimentally. The high 120
electronic densities of WDM make it opaque to optical probes, and 121
therefore, hard x-rays of keV energy are required to access the bulk 122
volume. 123

124 As a further development of pioneering experiments using laser-
125 based x-ray sources, the advent of x-ray free-electron lasers has
126 matured enough to provide revolutionary capabilities in the diagnosis
127 of dynamically compressed matter, mainly created by high energy
128 lasers producing compression waves on nanosecond timescales.
129 Methods applied include spectrally resolved x-ray Thomson scattering
130 (XRTS) that can access the electron temperature and density, the ioni-
131 zation state, and plasmon features. The plasmon feature is sensitive to
132 frequency-dependent electron–ion collision processes, which are
133 related to the electrical conductivity.³⁷

134 In this work, we present high-resolution x-ray scattering mea-
135 surements obtained in the collective regime from undriven carbon
136 samples in comparison with theoretical predictions using the time-
137 dependent density functional theory (TDDFT).³⁸ Furthermore, the
138 possibility of observing the C–H demixing and hydrogen metallization
139 via plasmon scattering under high pressure and high temperature is
140 investigated with the help of experiments including a rep-rated ener-
141 getic shock driver. 141

142 II. X-RAY THOMSON SCATTERING

143 X-ray Thomson scattering is an established diagnostic method
144 for characterizing WDM.^{39,40} The particular experimental setup used
145 illuminated sample by a linearly polarized x-ray free-electron laser in
146 the horizontal plane. The incident wave vector \mathbf{k}_0 is described with
147 $k_0 = 2\pi E_0/hc$. The scattered radiation is observed at the scattering
148 angle θ along the direction of the scattered wave vector \mathbf{k}_s above the
149 sample by a spectrometer. The scattering vector \mathbf{k} is defined by $\mathbf{k} = \mathbf{k}_s$
150 $- \mathbf{k}_0$. For small momentum and energy transfers from the incident x-
151 ray photon to the electron ($\hbar\omega \ll \hbar\omega_0$, where ω_0 denotes the fre-
152 quency of the incident radiation), the magnitude of the incident wave
153 vector is close to the scattered wave vector, $k_0 \approx k_s$, and the absolute
154 value of the scattering vector k can be determined by

$$k = |\mathbf{k}| = 4\pi \frac{E_0}{hc} \sin\left(\frac{\theta}{2}\right). \quad (1)$$

155 The collective and non-collective regimes are distinguished by
156 the scattering parameter $\alpha = 1/k\lambda_s$, where λ_s is the plasma screening

length: $\alpha \geq 1$ corresponds to the collective scattering regime, and $\alpha \ll 1$ is characteristic for non-collective scattering. As α is dependent on k , different regimes can be accessed by varying the incident x-ray energy E_0 and/or the scattering angle θ . Here, the focus is on collective scattering to resolve plasmon oscillations of the electrons.

The obtained spectra can, then, be compared to models of the dynamic structure factor $S(k, \omega)$, which describes the scattering of radiation from charge density fluctuations. Theoretically, the dynamic structure factor can be obtained by the inversion of the total electronic dielectric function $\epsilon(\mathbf{k}, \omega)$. This expression is equivalent to the total electron density response function $\chi(\mathbf{k}, \omega)$.⁴¹ The dynamic structure factor is obtained using the fluctuation–dissipation theorem,⁴²

$$S(\mathbf{k}, \omega) = \frac{\hbar}{\pi n_e} \frac{1}{1 - e^{\hbar\omega/k_B T_e}} \text{Im}[\chi(\mathbf{k}, \omega)]. \quad (2)$$

For an advanced study of the sample properties, dynamic structure factor predictions can be extracted from state-of-the-art *ab initio* methods. For the study, time-dependent density functional theory (TDDFT) simulations⁴³ were performed. At ambient conditions, the linear-response TDDFT calculations were performed using the full-potential linearized augmented-plane wave code implemented in Elk⁴⁴ using bootstrap,⁴⁵ a long-range exchange–correlation (XC) kernel for TDDFT as implemented in the Elk code. The response functions at high-pressure and high-temperature conditions are evaluated using the adiabatic local density approximation for TDDFT in yambo⁴⁶ applying the Kohn–Sham⁴⁷ orbitals evaluated by Quantum ESPRESSO.⁴⁸ The simulations were performed for a system size ranging from 64 to 256 atoms consisting of C, H, CH, CH₃, and C₃H in a supercell using a $2 \times 2 \times 2$ k -point mesh. The Perdew–Burke–Ernzerhof (PBE)⁴⁹ XC functional is used in all the calculations.

185 III. RESULTS

The experimental data presented here were obtained at the High-Energy-Density (HED) instrument of the European X-ray Free-Electron Laser Facility (EuXFEL).⁵⁰ The setup used was typical for *in situ* x-ray diagnostics of laser-driven shock waves at XFEL facilities combining spectrally resolved x-ray scattering in both forward and backward geometries with x-ray diffraction, and only the drive laser was not yet available. The details of the setup together with an analysis of the backward scattering data have been described by Voigt *et al.*⁵¹ For demonstrating the forward scattering capabilities, 10 μm thick diamond samples were probed by x-ray pulses with a photon energy of ~ 6000 eV, focused to $< 10 \mu\text{m}$ spot sizes using beryllium compound refractive lenses. A monochromator was used to reduce the energy bandwidth to ~ 1 eV, from originally ~ 20 eV corresponding to the self-amplified spontaneous-emission (SASE) bandwidth. Both the spectrometers used cylindrically bent Highly Annealed Pyrolytic Graphite (HAPG) crystals with 80 mm radius of curvature, albeit the crystals used in the forward scattering setups had coating thickness of 100 μm compared with 40 μm in the backward direction.⁵² The backward scattering setup had a JUNGFRAU detector⁵³ at 155, to study x-ray Raman spectroscopy from different samples.⁵¹ The forward scattering signal was collected on an ePix100 detector⁵⁴ at 18. Dark images were taken as an average of 1200 frames (corresponding to a 2 min 10 Hz acquisition) per gain mode. The setup also included an ePix100 detector for x-ray diffraction (XRD) and an Andor Zyla 5.5 sCMOS

detector along with a bent Si-111 crystal spectrometer downstream of transmitted x-rays to measure the source spectrum.⁵¹

For the analysis of the forward spectrometer, pixel values with less than a nominal threshold associated with a clear single photon hit were truncated to zero for reducing the noise. Pixel noise in high gain corresponds to ~ 290 eV, allowing us to identify single photon counts with only Poisson noise. Several thousand two-dimensional detector images were, then, summed up to derive a lineout. Figure 1 illustrates the forward scattering spectrum from a 10 μm thick diamond sample. The plasmon feature, in this case collective excitations of valence band electrons, is usually downshifted by ~ 30 eV with respect to the elastic peak.⁵⁵ Using the monochromator allows the plasmon feature and the substructures to be clearly resolved, which would have been smeared out with pure SASE.

The forward scattering angle and the XFEL photon energy result in an absolute value of the scattering vector of $\sim 0.94 \text{ \AA}^{-1}$ applying Eq. (1). This wave number was, then, used as input for generating synthetic spectra from TDDFT simulations. In Fig. 2, the plasmon feature obtained from the experiment is compared with the TDDFT simulations convolved with the experimental instrument function. The synthetic spectrum shows reasonable agreement with the experimental data, reproducing the detailed features, except the surface plasmon feature at ~ 25 eV,⁵⁶ which is not covered by the bulk nature of the simulations. The total energy resolution obtained using the monochromator with 100 μm HAPG crystals is ~ 5 eV. As the 100 μm HAPG crystals have more depth broadening than the 40 μm HAPG crystals that were used in the backward scattering setup of the same experiment, by using the 40 μm HAPG crystals in the forward scattering setup could bring down the total spectral resolution to ~ 3 eV.⁵² Solely using the SASE mode results in ~ 20 eV, which smears out all substructures of the plasmon feature and results in overlap with the elastic scattering peak. The lower signal due to the monochromator has been compensated by taking a larger number of shots cumulatively.

243 IV. DISCUSSION

The obtained results suggest the applicability of the method presented for observing C–H demixing and hydrogen metallization under

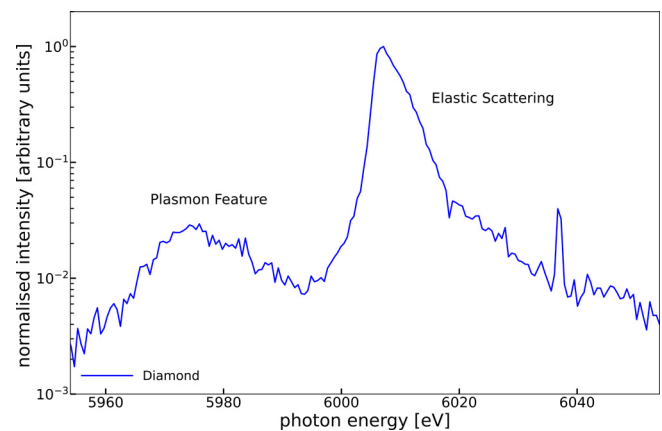


FIG. 1. Forward x-ray scattering spectrum from diamond, normalized to the maximum of the elastic signal peak. Spectra were obtained by averaging over 18 000 shots using the x-ray beam in the SASE configuration along with a monochromator. The plasmon feature is presented on a linear scale in Fig. 2.

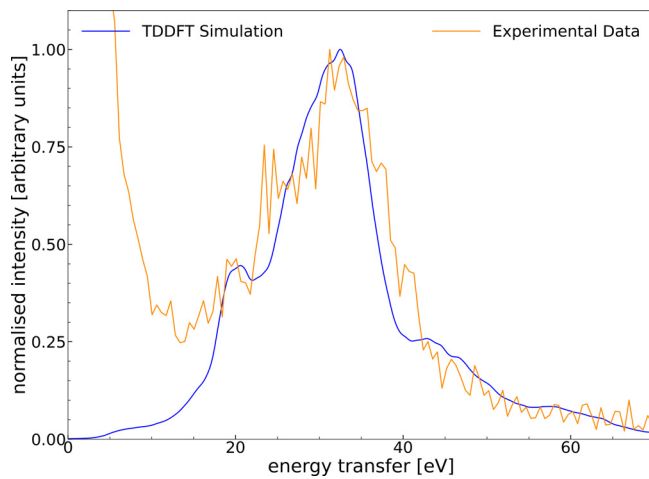


FIG. 2. Measured plasmon feature (orange) from Fig. 1 in comparison with the calculated plasmon feature (blue) after convolution with the instrument function.

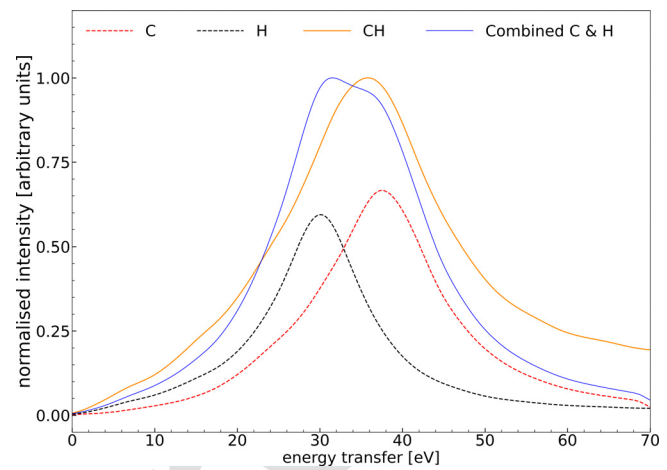


FIG. 3. Calculated spectra for CH in mixed state (orange) and demixed state (blue) for the scattering vector of $k = 0.94 \text{ \AA}^{-1}$. The demixed state plasmon is a combination of the characteristic carbon (red dotted) and metallic hydrogen (black dotted) features.

246 high-pressure, high-temperature conditions. In previous experiments,
 247 polystyrene (CH) samples were dynamically compressed at the Linac
 248 Coherent Light Source showing C–H phase separation on nanosecond
 249 timescales using *in situ* x-ray diffraction.^{24,57} Frydrych *et al.*⁵⁸ used
 250 a similar experimental setup to determine the degree of species separation
 251 in a dynamically compressed polystyrene sample to WDM conditions
 252 from spectrally resolved forward and backward x-ray scattering
 253 data. At pressures of the order of ~ 150 GPa and temperatures around
 254 ~ 6000 K, the carbon transforms into nanometer-sized diamonds.
 255 Measured diffraction lineouts provide indirect evidence for nearly
 256 complete C–H separation (REF—under way), where the isolated
 257 hydrogen would be expected to be in a liquid metallic state. However,
 258 as XRD does not provide a signal from the weakly scattering hydrogen,
 259 and reflectivity measurements from the compression fronts remain
 260 elusive due to the ongoing chemical reaction,⁵⁹ so far there is no direct
 261 evidence for the presence of liquid metallic hydrogen in these experi-
 262 ments. Due to its sensitivity to electronic structure and bulk conductiv-
 263 ity, the high-resolution forward scattering method described here can
 264 overcome these limitations and clarify the state of hydrogen in dynam-
 265 ically compressed C–H mixtures.

266 To test the sensitivity with the achieved spectral resolution,
 267 TDDFT calculations of the plasmon structures for C, H, and CH at
 268 conditions of $P \sim 150$ GPa and $T \sim 6000$ K were performed on ionic
 269 configurations obtained from density functional molecular dynamics
 270 (DFT-MD) simulations performed using VASP.^{60–63} For consistency,
 271 the TDDFT calculations of the dynamic structure factor were per-
 272 formed at the k -vector magnitude of $\sim 0.94 \text{ \AA}^{-1}$, i.e., the same as the
 273 forward scattering in the experiment. The spectral contributions of all
 274 three species were convolved with the experimentally obtained instru-
 275 ment function.⁵¹ The results are depicted in Fig. 3 and show a single
 276 peak with an almost Gaussian shape for a fully mixed CH sample. For
 277 fully demixed CH, a culmination of two distinctly shifted plasmon fea-
 278 tures from the two separate components is observed, forming a
 279 double-peak structure. The peak at higher energy shifts originates
 280 from the collective excitations of the diamond valence band, while the
 281 peak at lower energy shifts represents the plasmon feature of liquid

metallic hydrogen. With the experimentally demonstrated spectral res-
 282 olution of ~ 3 eV possible using the $40 \mu\text{m}$ HAPG crystals, and a sep-
 283 aration between the peaks of ~ 6 – 8 eV, C–H phase separation and
 284 hydrogen metallization can be observed using the demonstrated setup
 285 in future experiments adding a rep-rated drive laser.
 286

287 Additional TDDFT dynamic structure factor calculations were
 288 performed on pure H and C, as well as other C–H mixtures (CH,
 289 CH₃, and C₃H) at different scattering vectors to obtain the respective
 290 plasmon peaks and plasmon dispersion shifts. Figure 4 shows the plas-
 291 mon energy shifts for varying k -values for each species. The obtained
 292 results show that the separation between the features of the fully dem-
 293 ixed components as shown in Fig. 3 is larger at smaller scattering

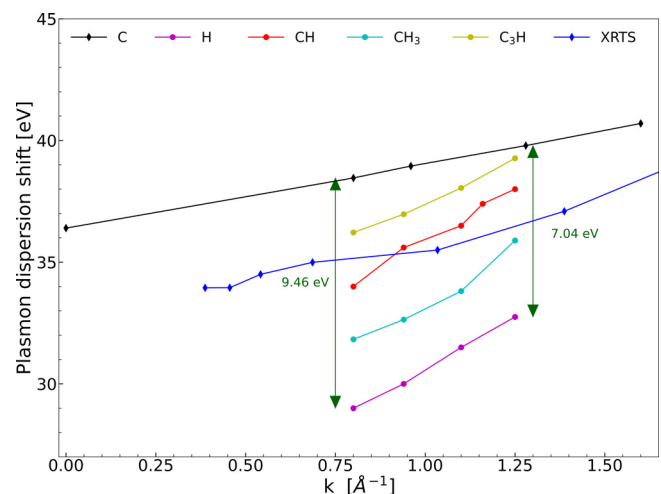


FIG. 4. Calculated plasmon energy shift for various species using the peak position of a respective plasmon in the forward scattering spectrum at different scattering vectors k . Plasmon shift in an experimental XRTS data at ambient conditions taken from Ref. 55 is also displayed for comparison.

294 vector magnitudes. The quadratic dispersion (shown up to $k \sim 1.60$)
 295 from the TDDFT results is weak, especially for carbon.^{43,55} The
 296 remaining results exhibiting a slightly stronger quadratic dispersion
 297 are only shown for $k = 0.80\text{--}1.25 \text{ \AA}^{-1}$ highlighting the spectral resolu-
 298 tion in the plasmon peaks required for diagnostics. In addition, the
 299 dispersion feature obtained using XRTS⁵⁵ for diamond at ambient
 300 conditions is additionally shown for Ref. 55 highlighting the differ-
 301 ences expected between ambient and warm dense carbon states. Thus,
 302 the corresponding experiments need to aim for small scattering angles
 303 and/or low photon energies to optimize the sensitivity for C–H separa-
 304 tion and hydrogen metallization via inelastic x-ray scattering.

305 In conclusion, the described method using collective x-ray
 306 Thomson scattering is applicable to characterize liquid metallic hydro-
 307 gen in the bulk of the sample, which is advantageous over the reflectiv-
 308 ity measurements that can only probe the surface (which may be in a
 309 non-equilibrium state, e.g., a shock front). We presented how the
 310 exemplar scattering spectrum from ambient diamond recorded at the
 311 HED instrument of European XFEL agrees well with the TDDFT sim-
 312 ulations performed. The existing resolution is capable of distinguishing
 313 the expected metallic hydrogen feature after demixing. In our demon-
 314 stration experiment, $\sim 18\,000$ shots were accumulated due to a signifi-
 315 cant decrease in x-ray flux due to the usage of a monochromator.
 316 With the new possibility to use self-seeded x-ray beams providing a
 317 spectral resolution comparable to using the monochromator,⁶⁴ but
 318 with approximately 50 times more x-ray photons per pulse, the
 319 required number of shots will be significantly reduced. Moreover, the
 320 samples applied in the demonstration experiment were notably thin-
 321 ner than those in typical shock-compression experiments at XFEL
 322 sources ($10 \mu\text{m}$ vs $50\text{--}100 \mu\text{m}$). Therefore, it can be expected that an
 323 accumulation of approximately 1000 shots or even less is required to
 324 obtain the data quality presented here. While high repetition rates
 325 place high demands on target design and the target delivery system,⁶⁵
 326 the corresponding developments are under way at the HED instru-
 327 ment, e.g., by allowing to replace targets without the need to break the
 328 vacuum in the interaction chamber.⁶⁶ Furthermore, plastics as a base
 329 target material allow for using tape samples that enable such rep-rated
 330 experiments with several 1000s of shots before targets have to be
 331 swapped.⁶⁷ Novel diagnostic tools combined with the new DiPOLE
 332 high-energy laser system at the HED instrument of EuXFEL will
 333 enable bulk-sensitive measurements of planetary core conditions. It is
 334 up to 10 Hz repetition rate, and pulse shaping capabilities⁶⁸ can be
 335 expected to play a crucial role in unlocking the physics behind the
 336 planets in the Solar System as well as the evolution of the steadily
 337 increasing number of confirmed exoplanets beyond.

339 ACKNOWLEDGMENTS

340 K.V., N.J.H., O.S.H., A.K.S., and D.K. were supported by the
 341 Helmholtz Association under VH-NG-1141, and O.S.H. was supported
 342 by the Helmholtz Association under Grant No. ERC-RA-0041. M.S.
 343 was supported by the Helmholtz Association under Grant No. VH-
 344 NG-1338. K.R. acknowledges funding by the Center for Advanced
 345 Systems Understanding (CASUS), which is financed by the German
 346 Federal Ministry of Education and Research (BMBF) and by the Saxon
 347 Ministry for Science, Culture and Tourism (SMWK) with tax funds on
 348 the basis of the budget approved by the Saxon State Parliament. The
 349 work of J.L. has been supported by GSI Helmholtzzentrum für

Schwerionenforschung, Darmstadt as part of the R&D project GSI-
 URDK2224 with the University of Rostock. N.J.H. and L.B.F. 350
 acknowledge support from the Department of Energy, Office of 351
 Science, Office of Fusion Energy Sciences, under FWP 100182, and 352
 N.J.H. was supported by the Department of Energy, Laboratory 353
 Directed Research, and Development program at SLAC National 354
 Accelerator Laboratory, under Contract No. DE-AC02-76SF00515. 355
 The work of S.P.H.-R. was performed under the auspices of the U.S. 356
 Department of Energy by Lawrence Livermore National Laboratory 357
 under Contract No. DEAC52-07NA27344. Computations were 358
 performed on a Bull Cluster at the Center for Information Services and 359
 High-Performance Computing (ZIH) at Technische Universität 360
 Dresden and on the cluster Hemera at Helmholtz-Zentrum Dresden- 361
 Rossendorf (HZDR). 362
 363
 364

AUTHOR DECLARATIONS

Conflict of Interest

The authors have no conflicts to disclose.

Author Contributions

Divyanshu Ranjan: Formal analysis (equal); Investigation (equal);
 Methodology (equal); Resources (equal); Writing – original draft
 (equal); Writing – review & editing (equal). **Samuel Schumacher:**
 Validation (equal); Writing – review & editing (equal). **Philipp**
Thomas May: Writing – review & editing (equal). **Alexis Amouretti:**
 Data curation (equal). **Karen Appel:** Data curation (equal). **Erik**
Brambrink: Data curation (equal). **Valerio Cerantola:** Data curation
 (equal). **Deniza Chekrygina:** Data curation (equal). **Luke Bennett**
Fletcher: Data curation (equal). **Sebastian Göde:** Data curation
 (equal). **Marion Harmand:** Data curation (equal). **Kushal rama-**
krishna: Data curation (equal); Formal analysis (equal); Investigation
 (equal); Resources (equal); Validation (equal); Writing – review &
 editing (equal). **Nicholas J. Hartley:** Data curation (equal); Writing –
 review & editing (equal). **Stefan P. Hau-Riege:** Data curation (equal).
Mikako Makita: Data curation (equal). **Alexander Pelka:** Data cura-
 tion (equal). **Anja Katharina Schuster:** Data curation (equal). **Michal**
Šmíd: Data curation (equal). **Toma Toncian:** Data curation (equal).
Min Zhang: Data curation (equal); Resources (equal). **Thomas**
Robert Preston: Data curation (equal); Writing – review & editing
 (equal). **Ulf Zastra:** Data curation (equal). **Katja Voigt:** Data cura-
 tion (equal); Methodology (equal); Resources (equal). **Jan Vorberger:**
 Formal analysis (equal); Resources (equal); Software (equal);
 Validation (equal); Writing – review & editing (equal). **Dominik**
Kraus: Conceptualization (equal); Data curation (equal); Formal anal-
 ysis (equal); Investigation (equal); Methodology (equal); Project
 administration (equal); Resources (equal); Supervision (equal);
 Validation (equal); Visualization (equal); Writing – review & editing
 (equal). **Oliver S. Humphries:** Data curation (equal); Methodology
 (equal); Resources (equal); Software (equal); Validation (equal);
 Writing – review & editing (equal). **Benjamin Heuser:** Validation
 (equal); Writing – review & editing (equal). **Michael Gareth**
Stevenson: Supervision (equal); Writing – review & editing (equal).
Julian Lüttger: Validation (equal); Writing – review & editing
 (equal). **Zhiyu He:** Validation (equal); Writing – review & editing
 (equal). **Chongbing Qu:** Validation (equal); Writing – review & edit-
 ing (equal).

406 DATA AVAILABILITY

407 The data that support the findings of this study are available
408 from the corresponding authors upon reasonable request.

409 REFERENCES

- 410 ¹A. Wolszczan and D. A. Frail, "A planetary system around the millisecond pulsar PSR1257 + 12," *Nature* **355**, 145–147 (1992).
- 411
- 412 ²M. Mayor and D. Queloz, "A Jupiter-mass companion to a solar-type star," *Nature* **378**, 355–359 (1995).
- 413
- 414 ³See https://exoplanetarchive.ipac.caltech.edu/docs/counts_detail.html for
415 "Exoplanet and Candidate Statistics, NASA Exoplanet Archive" (accessed
416 March 20, 2022).
- 417 ⁴See <https://exoplanetarchive.ipac.caltech.edu/exoplanetplots/> for "Exoplanet
418 Pre-Generated plots, NASA Exoplanet Archive" (accessed March 20, 2022).
- 419 ⁵W. Borucki, "KEPLER Mission: Development and overview," *Rep. Prog. Phys.* **79**, 036901 (2016).
- 420
- 421 ⁶T. Guillot, "Interiors of giant planets inside and outside the solar system," *Science* **286**, 72–77 (1999).
- 422
- 423 ⁷R. Chau, S. Hamel, and W. Nellis, "Chemical processes in the deep interior of Uranus," *Nat. Commun.* **2**, 203 (2011).
- 424
- 425 ⁸S. Lobanov, P. Chen, X.-J. Chen, C.-S. Zha, K. Litsov, and A. Goncharov, "Carbon precipitation from heavy hydrocarbon fluid in deep planetary interiors," *Nat. Commun.* **4**, 2446 (2013).
- 426
- 427 ⁹F. Graziani, M. Desjarlais, R. Redmer, and S. Trickey, *Frontiers and Challenges in Warm Dense Matter* (2014).
- 428
- 429 ¹⁰M. Bonitz, T. Dornheim, Z. A. Moldabekov, S. Zhang, P. Hamann, H. Kählert, A. Filinov, K. Ramakrishna, and J. Vorberger, "Ab initio simulation of warm dense matter," *Phys. Plasmas* **27**, 042710 (2020).
- 430
- 431 ¹¹E. Wigner and H. B. Huntington, "On the Possibility of a Metallic Modification of Hydrogen," *J. Chem. Phys.* **3**, 764–770 (1935).
- 432
- 433 ¹²L. Landau and Y. B. Zeldovich, "On the relation between the liquid and the gaseous states of metals," *Acta Physicochim. USSR* **18**, 194–196 (1943).
- 434
- 435 ¹³N. W. Ashcroft, "Metallic hydrogen: A high-temperature superconductor?," *Phys. Rev. Lett.* **21**, 1748–1749 (1968).
- 436
- 437 ¹⁴S. A. Bonev, E. Schwegler, T. Ogitsu, and G. Galli, "A quantum fluid of metallic hydrogen suggested by first-principles calculations," *Nature* **431**, 669–672 (2004).
- 438
- 439 ¹⁵V. E. Fortov, R. I. Ilkaev, V. A. Arinin, V. V. Burtzev, V. A. Golubev, I. L. Iosilevskiy, V. V. Khrustalev, A. L. Mikhailov, M. A. Mochalov, V. Y. Ternovoi, and M. V. Zhernokletov, "Phase transition in a strongly nonideal deuterium plasma generated by quasi-isentropic compression at megabar pressures," *Phys. Rev. Lett.* **99**, 185001 (2007).
- 440
- 441 ¹⁶S. Scandolo, "Liquid-liquid phase transition in compressed hydrogen from first-principles simulations," *Proc. Natl. Acad. Sci. U. S. A.* **100**, 3051–3053 (2003).
- 442
- 443 ¹⁷M. A. Morales, C. Pierleoni, E. Schwegler, and D. M. Ceperley, "Evidence for a first-order liquid-liquid transition in high-pressure hydrogen from ab initio simulations," *Proc. Natl. Acad. Sci. U. S. A.* **107**, 12799–12803 (2010).
- 444
- 445 ¹⁸T. Guillot, "The interiors of giant planets: Models and outstanding questions," *Annu. Rev. Earth Planet. Sci.* **33**, 493–530 (2005).
- 446
- 447 ¹⁹W. B. Hubbard, W. J. Nellis, A. C. Mitchell, N. C. Holmes, S. S. Limaye, and P. C. McCandless, "Interior structure of Neptune: Comparison with Uranus," *Science* **253**, 648–651 (1991).
- 448
- 449 ²⁰R. Helled, J. D. Anderson, M. Podolak, and G. Schubert, "Interior models of Uranus and Neptune," *Astrophys. J.* **726**, 15 (2010).
- 450
- 451 ²¹N. Nettelmann, K. Wang, J. Fortney, S. Hamel, S. Yellamilli, M. Bethkenhagen, and R. Redmer, "Uranus evolution models with simple thermal boundary layers," *Icarus* **275**, 107–116 (2016).
- 452
- 453 ²²H. Hirai, K. Konagai, T. Kawamura, Y. Yamamoto, and T. Yagi, "Polymerization and diamond formation from melting methane and their implications in ice layer of giant planets," *Phys. Earth Planet. Inter.* **174**, 242–246 (2009).
- 454
- 455 ²³M. Ross, "The ice layer in Uranus and Neptune-diamonds in the sky?," *Nature* **292**, 435–436 (1981).
- 456
- 457 ²⁴D. Kraus, N. Hartley, S. Frydrych, A. Schuster, K. Rohatsch, M. Rödel, T. Cowan, S. Brown, E. Cunningham, T. Driel, L. Fletcher, E. Galtier, E. Gamboa, A. Laso Garcia, D. Gericke, E. Granados, P. Heimann, H. Lee, M. MacDonald, and J. Vorberger, "High-pressure chemistry of hydrocarbons relevant to planetary interiors and inertial confinement fusion," *Phys. Plasmas* **25**, 056313 (2018).
- 458
- 459 ²⁵L. Benedetti, J. Nguyen, W. Caldwell, H. Liu, M. Kruger, and R. Jeanloz, "Dissociation of CH₄ at high pressures and temperatures: Diamond formation in giant planet interiors?," *Science* **286**, 100–102 (1999).
- 460
- 461 ²⁶Z. He, M. Rödel, J. Lüttger, A. Bergermann, M. Bethkenhagen, D. Chekrygina, T. E. Cowan, A. Descamps, M. French, E. Galtier, A. E. Gleason, G. D. Glenn, S. H. Glenzer, Y. Inubushi, N. J. Hartley, J.-A. Hernandez, B. Heuser, O. S. Humphries, N. Kamimura, K. Katagiri, D. Khaghani, H. J. Lee, E. E. McBride, K. Miyanishi, B. Nagler, B. Ofori-Okai, N. Ozaki, S. Pandolfi, C. Qu, D. Ranjan, R. Redmer, C. Schoenwaelder, A. K. Schuster, M. G. Stevenson, K. Sueda, T. Togashi, T. Vinci, K. Voigt, J. Vorberger, M. Yabashi, T. Yabuuchi, L. M. V. Zinta, A. Ravasio, and D. Kraus, "Diamond formation kinetics in shock-compressed C–H–O samples recorded by small-angle x-ray scattering and x-ray diffraction," *Sci. Adv.* **8**, eabo0617 (2022).
- 462
- 463 ²⁷M. Murillo, "Strongly coupled plasma physics and high energy-density matter," *Phys. Plasmas* **11**, 2964–2971 (2004).
- 464
- 465 ²⁸D. Riley, "Generation and characterisation of warm dense matter with intense lasers," *Plasma Phys. Controlled Fusion* **60**, 1–11 (2017).
- 466
- 467 ²⁹M. Eremets and I. Troyan, "Conductive dense hydrogen," *Nat. Mater.* **10**, 927–931 (2011).
- 468
- 469 ³⁰R. P. Dias and I. F. Silvera, "Observation of the Wigner-Huntington transition to metallic hydrogen," *Science* **355**, 715–718 (2017).
- 470
- 471 ³¹I. Silvera, R. Husband, A. Salamat, and M. Zaghoo, "Expanded comment on: optical properties of fluid hydrogen at the transition to a conducting state," *Nat. Mater.* **15**, 1000 (2016).
- 472
- 473 ³²P. Loubeyre, F. Occelli, and P. Dumas, "Synchrotron infrared spectroscopic evidence of the probable transition to metal hydrogen," *Nature* **577**, 631–635 (2020).
- 474
- 475 ³³M. Knudson, M. Desjarlais, A. Becker, R. Lemke, K. Cochran, M. Savage, D. Bliss, T. Mattsson, and R. Redmer, "High-pressure physics. Direct observation of an abrupt insulator-to-metal transition in dense liquid deuterium," *Science* **348**, 1455–1460 (2015).
- 476
- 477 ³⁴P. Celliers, M. Millot, S. Brygoo, R. McWilliams, D. Fratanduono, J. Rygg, A. Goncharov, P. Loubeyre, J. Eggert, L. Peterson, N. Meezan, S. Pape, G. Collins, R. Jeanloz, and R. Hemley, "Insulator-metal transition in dense fluid deuterium," *Science* **361**, 677–682 (2018).
- 478
- 479 ³⁵S. Weir, A. Mitchell, and W. Nellis, "Metallization of Fluid Molecular Hydrogen at 140 GPa (1.4 Mbar)," *Phys. Rev. Lett.* **76**, 1860–1863 (1996).
- 480
- 481 ³⁶P. Davis, T. Döppner, J. Rygg, C. Fortmann, L. Divol, A. Pak, L. Fletcher, A. Becker, B. Holst, P. Sperling, R. Redmer, M. Desjarlais, P. Celliers, G. Collins, O. Landen, R. Falcone, and S. Glenzer, "X-ray scattering measurements of dissociation-induced metallization of dynamically compressed deuterium," *Nat. Commun.* **7**, 11189 (2016).
- 482
- 483 ³⁷P. Sperling, E. Gamboa, H. Lee, H. Chung, E. Galtier, Y. Omarbakiyeva, H. Reinholz, G. Roepke, U. Zastra, J. Hastings, L. Fletcher, and S. Glenzer, "Free-electron x-ray laser measurements of collisional-damped plasmons in isochorically heated warm dense matter," *Phys. Rev. Lett.* **115**, 115001 (2015).
- 484
- 485 ³⁸M. Marques and E. Gross, "Time-dependent density functional theory," *Annu. Rev. Phys. Chem.* **55**, 427–455 (2004).
- 486
- 487 ³⁹A. Kritcher, P. Neumayer, H. Lee, T. Döppner, R. Falcone, S. Glenzer, and E. Morse, "Demonstration of x-ray Thomson scattering using picosecond k- α x-ray sources in the characterization of dense heated matter," *Rev. Sci. Instrum.* **79**, 10E739–10E739 (2008).
- 488
- 489 ⁴⁰S. H. Glenzer, W. Rozmus, B. J. MacGowan, K. G. Estabrook, J. D. D. Groot, G. B. Zimmerman, H. A. Baldis, J. A. Harte, R. W. Lee, E. A. Williams, and B. G. Wilson, "Thomson scattering from high-Z laser-produced plasmas," *Phys. Rev. Lett.* **82**, 97–100 (1999).
- 490
- 491 ⁴¹S. H. Glenzer and R. Redmer, "X-ray Thomson scattering in high energy density plasmas," *Rev. Mod. Phys.* **81**, 1625–1663 (2009).
- 492
- 493 ⁴²R. Kubo, "The fluctuation-dissipation theorem," *Rep. Prog. Phys.* **29**, 255 (1966).
- 494
- 495 ⁴³K. Ramakrishna and J. Vorberger, "Ab initio dielectric response function of diamond and other relevant high pressure phases of carbon," *J. Phys.: Condens. Matter* **32**, 095401 (2019).

AQ3

AQ2

AQ4

AQ6

537 ⁴⁴See <http://elk.sourceforge.net/> for “ELK, all-electron full-potential linearised
538 augmented plane wave (FP-LAPW) code” (2022).

539 ⁴⁵S. Sharma, J. Dewhurst, A. Sanna, and E. Gross, “Bootstrap approximation for
540 the exchange-correlation kernel of time-dependent density-functional theory,”
541 *Phys. Rev. Lett.* **107**, 186401 (2011).

542 ⁴⁶A. Marini, C. Hogan, M. Gruening, and D. Varsano, “yambo: An ab initio tool
543 for excited state calculations,” *Comput. Phys. Commun.* **180**, 1392–1403
544 (2009).

545 ⁴⁷W. Kohn and L. J. Sham, “Self-consistent equations including exchange and
546 correlation effects,” *Phys. Rev.* **140**, A1133–A1138 (1965).

547 ⁴⁸P. Giannozzi, O. Andreussi, T. Brumme, O. Bunau, M. B. Nardelli, M.
548 Calandra, R. Car, C. Cavazzoni, D. Ceresoli, M. Cococcioni *et al.*, “Advanced
549 capabilities for materials modelling with Quantum ESPRESSO,” *J. Phys. Matter*
550 **29**, 465901 (2017).

551 ⁴⁹J. P. Perdew, K. Burke, and M. Ernzerhof, “Generalized gradient approximation
552 made simple,” *Phys. Rev. Lett.* **77**, 3865 (1996).

553 ⁵⁰M. Nakatsutsumi, K. Appel, G. Priebe, I. Thorpe, A. Pelka, B. Muller, and T.
554 Tschentscher, “Scientific Instrument High Energy Density Physics (HED),” ■
555 (2014).

556 ⁵¹K. Voigt, M. Zhang, K. Ramakrishna, A. Amouretti, K. Appel, E. Brambrink, V.
557 Cerantola, D. Chekrygina, T. Döppner, R. Falcone, K. Falk, L. Fletcher, D.
558 Gericke, S. Göde, M. Harmand, N. Hartley, S. Hau-Riege, L.-G. Huang, O.
559 Humphries, and D. Kraus, “Demonstration of an x-ray Raman spectroscopy
560 setup to study warm dense carbon at the high energy density instrument of
561 European XFEL,” *Phys. Plasmas* **28**, 082701 (2021).

562 ⁵²T. Preston, S. Göde, J.-P. Schwinkendorf, K. Appel, E. Brambrink, V.
563 Cerantola, H. Höppner, M. Makita, A. Pelka, C. Prescher, K. Sukharnikov, A.
564 Schmidt, I. Thorpe, T. Toncian, A. Amouretti, D. Chekrygina, R. Falcone, K.
565 Falk, L. Fletcher, E. Galtier, M. Harmand, N. Hartley, S. Hau-Riege, P.
566 Heimann, L. Huang, O. Humphries, O. Karnbach, D. Kraus, H. Lee, B. Nagler,
567 S. Ren, A. Schuster, M. Smid, K. Voigt, M. Zhang, and U. Zastra, “Design and
568 performance characterisation of the HAPG von Hámos spectrometer at the
569 high energy density instrument of the European XFEL,” *J. Instrumentation* **15**,
570 P11033 (2020).

571 ⁵³A. Mozzanica, A. Bergamaschi, M. Brueckner, S. Cartier, R. Dinapoli, D.
572 Greiffenberg, J. Jungmann-Smith, D. Maliakal, D. Mezza, M. Ramilli, C. Ruder,
573 L. Schaedler, B. Schmitt, X. Shi, and G. Tinti, “Characterization results of the
574 JUNGFRÄU full scale readout ASIC,” *J. Instrumentation* **11**, C02047–C02047
575 (2016).

576 ⁵⁴K. Nishimura, G. Blaj, P. Caragiulo, G. Carini, A. Dragone, G. Haller, P. Hart,
577 J. Hasi, R. Herbst, S. Herrmann, C. Kenney, M. Kwiatkowski, B. Markovic, S.
578 Osier, J. Pines, B. Reese, J. Segal, A. Tomada, and M. Weaver, “Design and per-
579 formance of the ePix camera system,” *AIP Conf. Proc.* **1741**, 040047 (2016).

580 ⁵⁵E. Gamboa, L. Fletcher, H. Lee, M. MacDonald, U. Zastra, M. Gauthier, D.
581 Gericke, J. Vorberger, E. Granados, J. Hastings *et al.*, “Band gap opening in
582 strongly compressed diamond observed by x-ray energy loss spectroscopy,”
583 Technical Report No. ■ (SLAC National Accelerator Laboratory, Menlo Park,
584 CA, 2016).

585 ⁵⁶L. Bursill, J. Peng, and S. Praver, “Plasmon response and structure of nano-
586 crystalline diamond powder,” *Philos. Mag. A* **76**, 769–781 (1997).

587 ⁵⁷D. Kraus, J. Vorberger, A. Pak, N. Hartley, L. Fletcher, S. Frydrych, E. Galtier,
588 E. Gamboa, D. Gericke, S. Glenzer, E. Granados, M. MacDonald,
A. Mackinnon, E. McBride, I. Nam, P. Neumayer, M. Roth, A. Saunders, A. Schuster, and R. Falcone, “Formation of diamonds in laser-compressed hydrocarbons at planetary interior conditions,” *Nat. Astron.* **1**, 606–611 (2017).

⁵⁸S. Frydrych, J. Vorberger, N. Hartley, A. Schuster, K. Ramakrishna, A. Saunders, T. van Driel, R. Falcone, L. Fletcher, E. Galtier *et al.*, “Demonstration of x-ray Thomson scattering as diagnostics for miscibility in warm dense matter,” *Nat. Commun.* **11**, 2620 (2020).

⁵⁹N. Hartley, C. Zhang, X. Duan, L.-G. Huang, S. Jiang, Y. Li, L. Yang, A. Pelka, Z. Wang, J. Yang, and D. Kraus, “Dynamically pre-compressed hydrocarbons studied by self-impedance mismatch,” *Matter Radiat. Extremes* **5**, 028401 (2020).

⁶⁰G. Kresse and J. Hafner, “Ab initio molecular dynamics for liquid metals,” *Phys. Rev. B* **47**, 558–561 (1993).

⁶¹G. Kresse and D. Joubert, “From ultrasoft pseudopotentials to the projector augmented-wave method,” *Phys. Rev. B* **59**, 1758–1775 (1999).

⁶²G. Kresse and J. Furthmüller, “Efficiency of ab-initio total energy calculations for metals and semiconductors using a plane-wave basis set,” *Comput. Mater. Sci.* **6**, 15–50 (1996).

⁶³G. Kresse and J. Furthmüller, “Efficient iterative schemes for ab initio total-energy calculations using a plane-wave basis set,” *Phys. Rev. B* **54**, 11169–11186 (1996).

⁶⁴J. Amann, W. Berg, V. Blank, F. J. Decker, Y. Ding, P. Emma, Y. Feng, J. Frisch, D. Fritz, J. Hastings, Z. Huang, J. Krzywinski, R. Lindberg, H. Loos, A. Lutman, H. D. Nuhn, D. Ratner, J. Rzepliela, D. Shu, Y. Shvyd’ko, S. Spampinati, S. Stoupin, S. Terentyev, E. Trakhtenberg, D. Walz, J. Welch, J. Wu, A. Zholents, and D. Zhu, “Demonstration of self-seeding in a hard-x-ray free-electron laser,” *Nat. Photonics* **6**, 693–698 (2012).

⁶⁵I. Prencipe, J. Fuchs, S. Pascarelli, D. W. Schumacher, R. B. Stephens, N. B. Alexander, R. Briggs, M. Büscher, M. O. Cernaianu, A. Choukourou *et al.*, “Targets for high repetition rate laser facilities: Needs, challenges and perspectives,” *High Power Laser Sci. Eng.* **5**, e17 (2017).

⁶⁶U. Zastra, K. Appel, C. Baecht, O. Baehr, L. Batchelor, A. Berghäuser, M. Banjafar, E. Brambrink, V. Cerantola, T. E. Cowan, H. Damker, S. Dietrich, S. Di Dio Cafiso, J. Dreyer, H.-O. Engel, T. Feldmann, S. Findeisen, M. Foese, D. Fulla-Marsa, S. Göde, M. Hassan, J. Hauser, T. Herrmannsdörfer, H. Höppner, J. Kaa, P. Kaever, K. Knöfel, Z. Konöpková, A. Laso García, H.-P. Liermann, J. Mainberger, M. Makita, E.-C. Martens, E. E. McBride, D. Möller, M. Nakatsutsumi, A. Pelka, C. Plueckthun, C. Prescher, T. R. Preston, M. Röper, A. Schmidt, W. Seidel, J.-P. Schwinkendorf, M. O. Schoelmerich, U. Schramm, A. Schropp, C. Strohm, K. Sukharnikov, P. Talkovski, I. Thorpe, M. Toncian, T. Toncian, L. Wollenweber, S. Yamamoto, and T. Tschentscher, “The high energy density scientific instrument at the European XFEL,” *J. Synchrotron Radiat.* **28**, 1393–1416 (2021).

⁶⁷F. P. Condamine, N. Jourdain, J.-C. Hernandez, M. Taylor, H. Bohlin, A. Fajstavr, T. M. Jeong, D. Kumar, T. Laštovička, O. Renner, and S. Weber, “High-repetition rate solid target delivery system for PW-class laser-matter interaction at ELI Beamlines,” *Rev. Sci. Instrum.* **92**, 063504 (2021).

⁶⁸S. Banerjee, K. Ertel, P. D. Mason, P. J. Phillips, M. D. Vido, J. M. Smith, T. J. Butcher, C. Hernandez-Gomez, R. J. S. Greenhalgh, and J. L. Collier, “DiPOLE: A 10 J, 10 Hz cryogenic gas cooled multi-slab nanosecond Yb:YAG laser,” *Opt. Express* **23**, 19542–19551 (2015).

AQ5